

A shell model for the simulation of rhombohedral carbonate minerals and their point defects

DIANA K. FISLER,^{1,*} JULIAN D. GALE,² AND RANDALL T. CYGAN^{1,†}

¹Geochemistry Department, Sandia National Laboratories, Albuquerque, New Mexico 87185-0750, U.S.A.

²Department of Chemistry, Imperial College of Science, Technology, and Medicine, South Kensington, London, SW7 2AY, U.K.

ABSTRACT

The electronic polarization of oxygen ions has been explicitly incorporated in a shell model to better simulate the structure of calcite and related rhombohedral carbonate minerals. Pair-potentials for Ca^{2+} ions and C and O comprising the carbonate molecular ion were simultaneously fitted to experimental lattice, elastic, dielectric, and vibrational data for calcite, and the structure and elastic properties of aragonite. The resulting potential parameters for the CO_3^{2-} group were then transferred to models for the structures and bulk moduli of the carbonate minerals incorporating Mn, Fe, Mg, Ni, Zn, Co, Cd, and thus a fully consistent set of interaction parameters for calculating the properties of the carbonate minerals was obtained. Defect energies for doping the divalent cations into the calcite structure, and for calcium and carbonate ion vacancies were calculated. In addition, various disorder types for dolomite, including anti-site defects, stacking defects, and the energy related to increasing the Ca/Mg ratio in the dolomite structure were simulated. The theoretical enthalpy for dolomite ordering (34.4 kJ/mol) compares very well with experimental measurements.

INTRODUCTION

The value of atomistic simulations in the earth and materials sciences lies in demonstrating the mechanisms of atomistic processes, and extending this capability to evaluate material properties to regimes where direct laboratory measurements are difficult or impossible to perform. Knowledge of the transport properties of cations in carbonate minerals is necessary to evaluate order/disorder relations, deformation, and geothermometry, but slow transport rates and the decomposition of carbonate phases at high temperatures limit experimental evaluation. Although simulations do not replace careful experimental measurements, a well-parameterized atomistic model can provide a solid framework for evaluating mechanisms and predicting activation energies and rates for diffusion under conditions not accessible to the experimentalist. This study develops a fully consistent model of the carbonate minerals based upon a shell description of the electronic structure of the oxygen in the covalent CO_3^{2-} group. Ultimately, the model may be used to calculate chemical diffusion rates, phase relations, and surface reactivity.

The divalent cations Ca, Mg, Mn, Fe, Cd, Zn, Co, and Ni form stable carbonate phases of the calcite structure, respectively, calcite, magnesite, rhodochrosite, siderite, octavite, smithsonite, and cobalt and nickel carbonates. They share the

mathematically equivalent hexagonal or rhombohedral structures. The structure may also be regarded as being comprised of basal layers of metal cations and layers of planar CO_3^{2-} groups normal to the *c* axis. In the mixed metal cation dolomite structure, Ca^{2+} and Mg^{2+} preferentially occupy the alternate hexagonal basal planes and form calcium and magnesium layers. Larger cations such as Sr^{2+} , Pb^{2+} , and Ca^{2+} at higher pressures form the orthorhombic aragonite structure, also composed of ionic CO_3^{2-} units and the metal cations.

Previous molecular mechanics studies (Pavese et al. 1992; Dove et al. 1992; Catti et al. 1993; Catti and Pavese 1997) generally focused on parameterizing a model for only CaCO_3 . These studies included extensive testing of both rigid ion and shell models of the lattices of calcite and aragonite, and calculated basic properties such as elastic and optical properties, and isotope fractionation. Parker et al. (1993) used the atomistic model for calcite to examine surface precipitation and dissolution processes, an area of wide application for geologic problems involving the alteration and weathering of carbonate rocks such as limestone, dolomite, and marble.

By calculating the properties of most of the known divalent carbonate phases, we have created a general framework for interpreting a variety of bulk carbonate properties, and for beginning to address the problems of inhomogeneous zoning and dolomitization. The fully transferable potentials for the CO_3^{2-} group, in particular, lend a great deal of flexibility to the empirical models, such that substitution defect energies and disorder defect energies can be derived. Additionally, the models can be used to evaluate transition state geometries and predict Arrhenius activation energies for chemical diffusion in the carbonate phases (Fisler et al. 1998).

*Present address: Johns Manville Technical Center, 10100 W. Ute Avenue, P.O. Box 625005, Littleton, Colorado 80162-5005, U.S.A.

†E-mail: rtcygan@sandia.gov

THEORETICAL PROCEDURE

Interatomic energy and shell model

The simulations performed in this study use a modification of the Born model description of solids, which treats the ionic material as a collection of point ions with electrostatic (Coulombic) and short-range forces acting between them. The procedure is described at length elsewhere (Catlow and Mackrodt 1982). In brief, the different energy contributions for all ion-ion interactions of the crystal are summed out to a maximum cut-off of 15 Å for the short-range terms (if there is no C_6 term then these can be truncated at 10 Å with no significant loss of accuracy) whereas electrostatic interactions are partially performed in reciprocal space according to the Ewald method to ensure proper convergence (Tosi 1964). The electrostatic potential V_{ij}^{el} is inversely proportional to the distance between ions:

$$V_{ij}^{el}(r_{ij}) = e^2 Z_i Z_j / r_{ij} \quad (1)$$

where r_{ij} is the distance between ions having charge Z_i and Z_j , and e is the charge of an electron. The short-range potential V_{ij}^{sr} is expressed as a function of the interatomic distance based on the Buckingham functional form:

$$V_{ij}^{sr}(r_{ij}) = A_{ij} \exp(-r_{ij}/\rho_{ij}) - C_{ij} r_{ij}^{-6} \quad (2)$$

where A_{ij} , ρ_{ij} , and C_{ij} are the empirical parameters for the short-range attractive and van der Waals energies. The potential form differs from that usually used in the Born model in that electronic polarization of ions in the lattice is accounted for by the addition of charged shells (Dick and Overhauser 1958). The ion is therefore represented by a massless shell of charge Z_s and a core of charge Z_c , where $Z_s + Z_c$ equals the total charge of the ion. The total charge on each ion in these simulations is reduced from its formal ionic charge and the partial charge on each ion is a fitted parameter. The core and shell are coupled by a harmonic spring of analytical form $E^{pol} = 1/2 kX^2$, where X represents the separation distance of the shell and core of an ion. During the energy minimization calculations, the shell positions are allowed to relax about the ion core resulting in a dipole that mimics the electronic polarization. Shells are only included for describing the large polarization associated with the oxygen ions; all other atoms were represented by a rigid ion.

Calcium carbonate minerals

The empirical fitting of model parameters often leads to a non-unique set of values that can easily reproduce the lattice parameters for a given structure. However, it is much more desirable and accurate to incorporate as many high quality measurements of observable properties, such as elastic and dielectric constants, as possible in the fitting of the parameters to maximize transferability. The structures of calcite (rhombohedral CaCO_3) and aragonite (orthorhombic CaCO_3), the elastic, static and high frequency dielectric constants and vibrational frequencies of the carbonate deformation modes of calcite have been used to fit the potential parameters using the relaxed fitting algorithm (Gale 1996) in which the changes in the structural parameters on optimization are used to calculate the residual error.

The chief improvement of our model for calcium carbonate over the previous studies (Pavese et al. 1992; Dove et al. 1992; Catti et al. 1993; Parker et al. 1993) is recognizing that completely different interaction potentials are required between and within CO_3^{2-} molecular anions. Therefore, an intermolecular O-O Buckingham potential and an intramolecular O-O Buckingham potential have been defined. A three-body O-C-O term and a torsional O-C-O-O potential simulate additional interactions within the CO_3^{2-} molecular anion. A more extensive functional form for the oxygen core/shell spring constant by including a 4th order term has been used to accurately reproduce the vibrational frequencies in calcite, while predicting the relative stability of aragonite with respect to calcite which is critically dependant on the oxygen polarizability. All intramolecular potentials are defined to act between cores while intermolecular interactions act on shells, where applicable. Furthermore, all Coulomb interactions are excluded within molecules. Table 1 provides the values for the optimized interatomic potential parameters obtained through this process.

Simulations of the bulk structure of calcite (and metal-substituted derivatives) use the primitive rhombohedral cell, although lattice parameters are reported here in hexagonal coordinates as the two representations are mathematically equivalent. The aragonite and the Mg-rich huntite phases require an orthorhombic simulation cell. The computer program

TABLE 1. Interionic potentials obtained from fits to calcite and aragonite structures and properties

Potentials	A_{ij} (eV)	r_{ij} (Å)	C_{ij} eV (Å ⁶)	Cutoffs (Å)
Buckingham (intramolecular) O-O	4030.30	0.2455		0–2.5
Buckingham (intermolecular) O-O	79158.6	0.1983	21.844	0–15
Buckingham Ca-O	2154.06	0.2891		0–10
Buckingham Cd-O	4329.81	0.2563		0–10
Buckingham Mn-O	2000.94	0.2727		0–10
Buckingham Fe-O	2151.99	0.2651		0–10
Buckingham Zn-O	1029.39	0.2891		0–10
Buckingham Co-O	1095.60	0.2863		0–10
Buckingham Ni-O	1634.46	0.2666		0–10
Buckingham Mg-O	1039.59	0.2893		0–10

Notes: For Morse C-O, $D_0 = 5.0$ eV, $a = 2.5155$ Å, and $r_0 = 1.2025$ Å.

For spring O-O, $k_2 = 32.194$ eV/Å² and $k_4 = 10000$ eV/Å⁴.

For three body O-C-O (intramolecular), $k_2 = 1.7887$ eV/rad², and $\theta_0 = 120^\circ$.

For torsion O-C-O-O, $k = 0.1510$ eV and $n = -2$.

Partial charges are $Z_c = +1.3435$, $Z_{O-core} = +1.0185$, $Z_{O-shell} = -2.1330$, and $Z_{Ca} = +2.0000$.

GULP (Gale 1997) was used to first derive the potential parameters and then to perform the energy minimizations required for the bulk structural and defect calculations. Energy minimizations were performed at constant pressure allowing all individual ionic coordinates and lattice parameters to vary, while constraining the space group symmetry. Although the theoretical results reported here are 0 K calculations, in practice, thermal effects are effectively included in the interatomic potentials by fitting to room temperature experimental data.

Other rhombohedral carbonate minerals

There are few high quality measurements of the structural and physical properties for the other divalent carbonate phases. The interatomic potentials and charges for the carbonate anion group and the cation charge (+2) were held fixed for fitting to the structure and the bulk modulus for the other carbonate phases; the only degree of freedom for the fitting model was in the cation-oxygen Buckingham potential. Due to the non-directional nature of the metal cation as described by the Buckingham potential of Equation 2, there is no explicit term that addresses the d-electrons of the transition metal cations. The transition metal cations are represented as spherical rigid ions (no electronic polarization) as with Ca^{2+} and Mg^{2+} , and therefore magnetic effects are ignored. The data for the bulk moduli were obtained from Zhang and Reeder (1999). Finally, structures for dolomite [$\text{CaMg}(\text{CO}_3)_2$] and huntite [$\text{Mg}_3\text{Ca}(\text{CO}_3)_4$] were simulated, with no attempt to further optimize the potentials with respect to those observed structures.

Defect calculations

A large number of defect calculations have been performed on oxides and halides (e.g., Catlow and Mackrodt 1982; Mackrodt 1984). Defect calculations of covalent materials are significantly less straightforward, but in examining calcite we are able to treat the structure as a de facto ionic solid and create ionic defects involving the metal cation and the CO_3^{2-} molecular anion. Mott and Littleton (1938) demonstrated that the displacement around a defect may be treated mathematically as a combination of short range and long range displacement regions. In this formalism, the lattice energy will almost certainly converge, as is not always possible if all ionic displacements in the full lattice are allowed. The defect formation energy can then be calculated from the difference between the energies of the defective lattice and the perfect lattice. The size of region 1 (the atomistic region immediately surrounding the defect) is increased until the energy of the defect has converged satisfactorily. The techniques used in defect calculations resemble those used in bulk lattice simulations except for the high degree of distortion in the environment of the defect, and the fact that the calculation can use only point group symmetry, if any exists, in the defective region. Region 1 typically contains up to a few hundred atoms, and all coordinates of the ions in this region are explicitly allowed to relax. In region 2a, which may contain several thousands of atoms, the relaxation energy is calculated assuming that the ions respond harmonically about their lattice sites to the electrostatic forces due to the defect species. Beyond this in region 2b, the ions respond only to the total charge of the defect and the relaxation energy is calculated

implicitly by lattice summation techniques. We used the above procedure to examine a variety of point defects in the carbonate phases, and performed several preliminary evaluations of more complex defect aggregates.

RESULTS

Table 2 compares the properties of calcium carbonate used to develop the shell model potentials (Table 1) by the described procedure. Table 2 also reports measured properties that were not used in the fit for comparison with the calculated values, and calculated properties for which there are no reliable experimental data. The vibrational frequencies were calculated at the gamma point (zero wavevector) and therefore we do not report dispersion curves and TO-LO modes. For degenerate vibrational modes in calcite both calculated frequencies are reported. In principle, all of the vibrational modes of calcite and aragonite could be used in the parameterization procedure, but due to the cooperative motions of a large number of atoms in the low frequency region, and the uncertainty in assigning the eigenvalues for each experimental mode, we have chosen to rely on the high frequency localized modes of the carbonate ion. This ensures that the parameterization properly fits vibrational frequencies to the correct internal modes. The low frequencies that are primarily associated with Ca-O modes are incorporated in the model by fitting the elastic properties rather than the vibrational frequencies.

The lattice parameters differ from reported values by less than experimental error for calcite, and those for aragonite differ by less than 1% (see Table 2). The elastic constants for calcite are reproduced with a relative error of approximately 6.6% including those not used in the fitting procedure. The elastic constants of aragonite are reproduced with about the same accuracy as previously published rigid ion models (e.g., Pavese et al. 1992), with the most obvious failure in the off-diagonal C_{12} and C_{13} constants. The relatively poor agreement in these off-diagonal terms is related to several factors: the emphasis of parameterization in the weighting on the diagonal terms, the structure, and relative energies of the two phases; the relative inaccuracies in the experimental data for aragonite compared to calcite; and the relatively simple nature of the bonding model. Overall, the new shell model provides a significant improvement in the prediction of the second derivative properties, including the elastic and dielectric constants and the vibrational frequencies, compared to the previous models.

Structures of the carbonate minerals

The calculated lattice parameters for the end-member carbonates (used in the fit) differ from their measured lattice parameters by less than 1% (Table 3). The relative errors in lattice parameters for the divalent carbonates are all slightly smaller than the relative error (2.1%) for calcite lattice parameters by the rigid ion model of Pavese et al. (1992). Lattice parameters for dolomite and huntite differed from measured values by less than 2%, although no attempt was made to fit to those structures directly. The lattice energy generally increases with increasing ionic radius (Fig. 1). The minor deviations of the lattice energies from the trend are attributed to the anomalous experimental bulk moduli with respect to bond length (and ionic ra-

TABLE 2. Experimental and calculated properties of CaCO₃

	Aragonite			Calcite		
	Experimental	Calculated	Δ (%)	Experimental	Calculated	Δ (%)
Elastic Constants (GPa)						
C ₁₁	85.0†	89.9	6.5	145.7§	140.9	-3.3
C ₂₂	159.6†	155.3	-2.7			
C ₃₃	87.0†	104.2	20	85.3§	85.8	0.6
C ₄₄	42.7†	23.3	-45	33.4§	33.4	0.0
C ₅₅	41.3†	36.7	-11			
C ₆₆	25.6†	12.4	-52			
C ₁₂	15.9†*	48.0	>100	55.9§	63.7	14
C ₁₃	36.6†*	55.9	53	53.5§*	62.6	17
C ₁₄				-20.5§*	-19.5	-4.9
C ₂₃	2.0†*	54.7				
Static Dielectric						
ϵ_{11}^0		7.84		8.5	9.28	9.2
ϵ_{22}^0		22.48				
ϵ_{33}^0		8.26		8.0	8.30	3.7
High Frequency Dielectric						
ϵ_{11}^∞	2.86†*	3.05	6.6	2.75‡	2.69	-2.2
ϵ_{22}^∞	2.82†*	2.53	-10			
ϵ_{33}^∞	2.34†*	2.50	6.8	2.21‡	3.02	37
Vibrational frequencies (cm⁻¹)						
Asymmetric stretch (IR), ν_3	1473#	1500	1.8	1463#	1465 1573	3.8
Symmetric C-O stretch (Raman), ν_1	1086#	1124	3.5	1088#	1082 1091	-0.1
Torsional bending (IR), ν_2	873#	781	-11	881#	878 994	6.2
Stretch/bend (IR), ν_4	705#	627	-11	714#	612	-14

* Properties not used in the potential fitting.

† Experimental values from Hearmon (1946).

‡ Experimental values from Deer et al. (1966).

§ Experimental values from Dandekar and Ruoff (1968).

|| Experimental values from Kaye and Laby (1982).

Experimental values averaged from White (1974).

dus) observed by Zhang and Reeder (1999) and which were used in the parameterization. Simple variation of the cation-oxygen potential parameters failed to satisfactorily reproduce the exact trend in bulk moduli.

The lattice energy of aragonite is less exothermic per mole than calcite at ambient pressure, consistent with the metastability of aragonite at room pressure. A series of minimizations have been performed at increasing applied pressure for both cal-

cite and aragonite and the corresponding enthalpies determined. Because of the differing degrees of oxygen polarization in the two structures the enthalpy increases at different rates as a function of pressure and a transition from calcite to aragonite is predicted to occur at approximately 2.4 kbar consistent with experimental measurements (Crawford and Hoersch 1972).

Defect energies

The Mott-Littleton method requires that the defect energy has properly converged to a value consistent with an infinitely large region 1 volume. The energies for each type of defect (Table 4) demonstrate convergence to within 0.02 eV for substitutional defects (0.1 eV for vacancies) with an increase in the size of region 1 from 6 to 12 Å. Region 2a was held fixed at 20 Å; varying this radius had a negligible effect on the defect energy. Figure 2 includes two views of a calcium vacancy in calcite and shows the limiting extents of the different calculation regions. The expanded view (Fig. 2b) shows that the significant distortion due to a calcium vacancy reaches less than 10 Å into the surrounding crystal. Substitutional defects (e.g., Mn for Ca) show much less distortion of the calcite lattice. The amount of distortion around a calcium vacancy in calcite is quantified by comparing oxygen-oxygen distances in the vicinity of the defect with those in the perfect lattice (Fig. 3). The O-O distances within the carbonate anion near the defect are seen to contract, whereas the intermolecular distances are observed to expand and also exhibit a broader range of values.

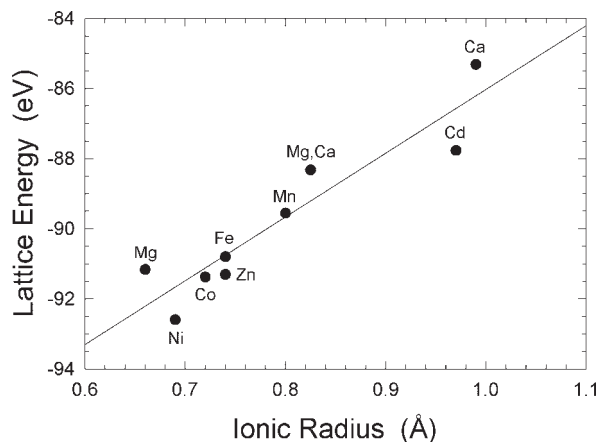


FIGURE 1. Calculated lattice energies for the rhombohedral carbonate minerals as a function of ionic radius of the divalent cation.

TABLE 3. Comparison of carbonate structural properties

Composition	Lattice energy (eV)	Bulk modulus			<i>a</i> (Å)	Δa (%)	<i>b</i> (Å)	Δb (%)	<i>c</i> (Å)	Δc (%)
		Calculated (GPa)	Experimental (GPa)	Δ (%)						
CaCO ₃ (calcite)‡	-85.31	77	73§§	5.5	4.99	0.01	4.99	17.06	-0.01	
CaCO ₃ (arag)†	-170.60	71	48##	47.9	5.75	0.31	4.94	7.92	0.61	
CaCO ₃ (arag)‡‡	-85.30									
CdCO ₃ §	-87.76	98	100*	-2.0	4.90	-0.51	4.90	16.39	-0.63	
MnCO ₃ ‡	-89.55	108	108*	0.0	4.78	0.29	4.78	15.56	-0.51	
FeCO ₃ ‡	-90.79	121	117*	3.4	4.73	0.80	4.73	15.25	-0.87	
ZnCO ₃ ‡	-91.30	123	123*	0.0	4.67	0.45	4.67	14.88	-0.94	
CoCO ₃	-91.37	124	124*	0.0	4.67	0.25	4.67	14.89	-0.51	
NiCO ₃	-92.59	138	131*	5.3	4.64	0.65	4.64	14.73	-0.03	
MgCO ₃ ‡	-91.16	122	107*	14.0	4.68	-0.96	4.68	14.92	0.69	
MgCa(CO ₃) ₂ **	-88.32	94	91*	3.3	4.85	0.89	4.85	15.82	-1.16	
½[Mg ₃ Ca(CO ₃) ₄]††	-179.68	110			9.64	1.40	9.64	7.70	-1.50	
½[Mg ₃ Ca(CO ₃) ₄]‡‡	-89.84									

* Bulk moduli from Zhang and Reeder (1999).

† Experimental lattice parameters from dal Negro and Ungaretti (1971).

‡ Experimental lattice parameters from Effenberger et al. (1981).

§ Experimental lattice parameters from Borodin et al. (1979).

|| Experimental lattice parameters from Graf (1961).

Experimental lattice parameters from Finger (1975).

** Experimental lattice parameters from Ross and Reeder (1992).

†† Experimental lattice parameters from Dollase and Reeder (1986).

‡‡ Aragonite and huntite are also reported per unit cell equivalent to the rhombohedral carbonates.

§§ Calculated from experimental elastic constants of Dandekar and Ruoff (1968).

Calculated from experimental elastic constants of Hearmon (1946).

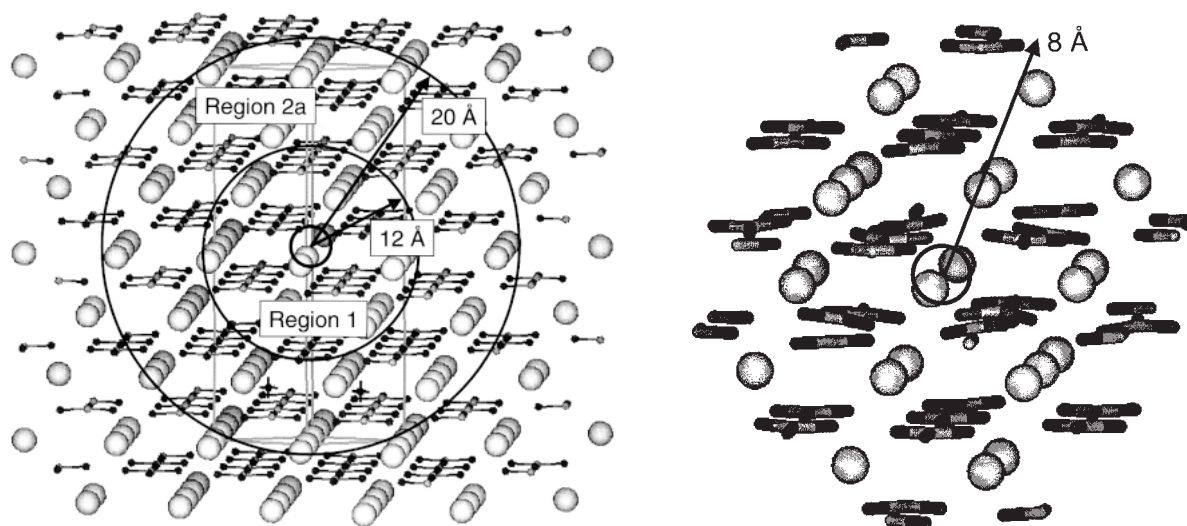


FIGURE 2. (a) Schematic of the defect region for a Ca vacancy in calcite based on the Mott-Littleton calculation method. The hexagonal-based unit cell of calcite is also indicated. Defect calculations were performed for region 1 radius varying from 6 to 12 Å. (b) Close-up view of an 8 Å defect region showing the distortion of CO₃²⁻ ions surrounding the calcium vacancy.

TABLE 4. Point defect energies (eV) in calcite as a function of region 1 radius

Defect	6 Å	8 Å	10 Å	12 Å
Ca vacancy V_{Ca}	20.71	20.52	20.43	20.53
CO ₃ vacancy V_{CO_3}	28.73	28.45	28.24	28.17
Schottky pair $V_{Ca} + V_{CO_3}$	46.776	30.478	46.378	not converged
Cd substitution Cd_{Ca}	-1.19	-1.19	-1.20	-1.20
Mn substitution Mn_{Ca}	-1.95	-1.99	-2.00	-2.01
Fe substitution Fe_{Ca}	-2.48	-2.53	-2.55	-2.56
Zn substitution Zn_{Ca}	-2.64	-2.71	-2.74	-2.76
Co substitution Co_{Ca}	-2.67	-2.75	-2.78	-2.79
Ni substitution Ni_{Ca}	-3.20	-3.29	-3.33	-3.35
Mg substitution Mg_{Ca}	-2.58	-2.65	-2.68	-2.70

Formation energies for Ca²⁺ and CO₃²⁻ vacancies are quite large and represent the energy for an isolated and charged vacancy defect being removed to an infinite distance from the crystal. Strictly, the energy for the vacancy defect should be calculated for removing the ion to the surface, though creating a surface was beyond the scope of the present study. Thus the calculated defect energies represent a maximum and should be compared to experimentally derived defect energies with caution. Also shown in Table 4 is the energy for a neutral Schottky defect pair of a Ca²⁺ vacancy and a CO₃²⁻ vacancy. The defect

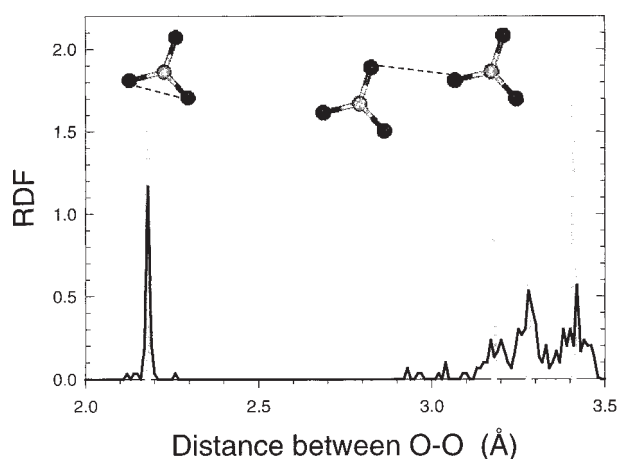


FIGURE 3. Radial distribution function (RDF) plot of the variation in oxygen-oxygen distance due to the presence of a calcium vacancy in calcite (black line) vs. that in the perfect lattice (gray line). Intramolecular O-O distances broaden in the defect region, whereas intermolecular oxygen-oxygen distances broaden and expand slightly. The dashed lines in the insets of the CO_3^{2-} groups represent the corresponding O-O distances for the peaks in the RDF.

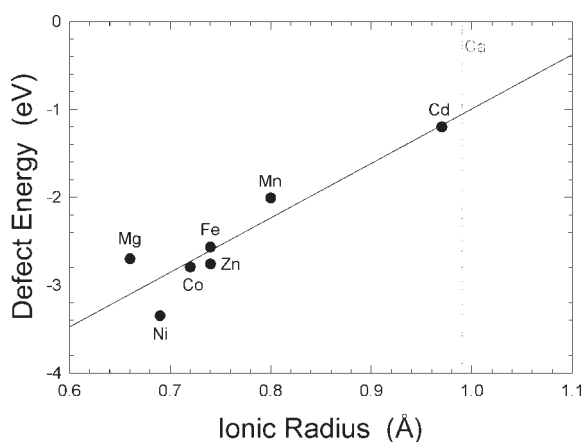


FIGURE 4. Substitution defect energies of metals in calcite as a function of ionic radius. Defect energies generally increase with decreasing metal radius.

was created by the removal of neighboring Ca^{2+} and CO_3^{2-} ions aligned along the c axis of the hexagonal cell and separated by a distance of 4.46 \AA . The results show that the formation energy for the coupled defect is less than the sum of the isolated defects. The reduced energy is related to the lattice distortion that occurs about the defect sites and the electrostatic interaction of the charged defect centers in forming an associated defect pair. Therefore, the long-range Coulombic contribution to the Schottky defect is approximately half the vacancy defect energy and the remainder of the energy is related to the accompanying steric distortion.

Defect calculations involving the substitution of other metal cations for Ca in calcite yield negative binding energies. The

spontaneous formation of these types of point defects results from their smaller ionic size. Defect energy of the metal substitution generally increases with the ionic radius of the metal ion (Fig. 4).

Dolomite disorder

Several different types of disorder associated with dolomite are easily addressed within the modeling framework and the new potential model. The energy of a single anti-site defect was calculated by combining a single substitution of magnesium for calcium paired with a substitution of calcium for magnesium. Stacking defect energies (Table 5) were determined from lattice energies of dolomite with a single magnesium and calcium site switched in a bulk supercell that is three times the unit-cell dimension in the c direction (total of 18 basal cation planes). To determine dolomite ordering energies, the occupancies of magnesium and calcium in the fully ordered dolomite unit cell were varied from 1 (fully ordered) to 0.5 (fully disordered). The lattice energies (Table 6) for the relaxed configurations representing this increasing disorder were calculated using a mean field approach in which each metal site of the dolomite experiences a potential that is the mean of all possible disordered positions. As a consequence, all possible configurations are equally as likely with no preference for any particularly stable configuration (Gale 1997). This modeling procedure also represents the carbonate configuration that would be expected to occur under kinetic control rather than a process that is driven by thermodynamics.

DISCUSSION

Bulk and defect structures

The models satisfactorily reproduce the lattice parameters and elastic properties of all the end-member rhombohedral carbonates and aragonite using a uniform set of potentials for the carbonate anion. However, less-satisfactory lattice parameters for dolomite and huntite result from the direct transfer of cation-oxygen potentials that were optimized for calcite and magnesite. In addition, the models have incorporated the unusually "soft" bulk modulus reported by Zhang and Reeder (1999) for magnesite. The experimental modulus is slightly smaller, yet similar to

TABLE 5. Energies for the formation of disordering defects in dolomite

Disorder types	Energy (eV)
$\text{Mg}_{\text{Ca}} + \text{Ca}_{\text{Mg}}$ anti-site defect	1.3
Stacking defect 1-1	0.505
Ca_{Mg}	5.03
Mg_{Ca}	-3.91

TABLE 6. Occupancy of calcium in calcium site as a function of lattice energy for dolomite at constant $\text{Ca}/\text{Mg} = 1$

Ca per Ca site	Lattice energy (eV)	Ca per Ca site	Lattice energy (eV)
1.00*	-88.32	0.75	-87.77
0.95	-88.18	0.65	-87.66
0.90	-88.05	0.60	-87.63
0.85	-87.94	0.50†	-87.60
0.80	-87.85		

*Fully ordered dolomite.

†Fully disordered dolomite.

the values obtained by Ross (1997) and Fiquet and Reynard (1999). Further refinement of these carbonate models may help to determine the source of the anomaly, in particular, further exploration of the specific properties of magnesite may allow calculation of the predicted changes in elastic properties with increasing substitutions and defects in the magnesite structure.

Understanding of the point defect structure of minerals is crucial in the characterization and evaluation of many chemical and physical properties. Kronenberg et al. (1984) indicated that manganese impurities are the mostly likely defect in calcite, and, indeed, all of the divalent cations are soluble in calcite up to a few percent. The present calculations indicate that the most favored impurity defect in calcite is Ni^{2+} . However, all substitutions occur as spontaneous defects, and the likelihood of a defect will obviously be dependent on the relative energy of competing metal oxides and on the availability of the cation dopant. The defect calculations also assume the existence of an isolated and uncharged defect. As the impurity content increases, this dilute defect approximation is no longer valid and the carbonate structure begins to markedly distort giving rise to two-phase regions. Electrical conductivity measurements by Rao and Rao (1968) indicate that lattice defects are responsible for charge transport in calcite, and they calculated formation energies between 1 and 2 eV. Although the defect structure of calcite is likely to be quite complex, the high formation energies calculated here for calcium vacancies imply that calcium vacancies alone are not responsible for transporting charge, and that extrinsic defects are likely to be involved in the formation of defects in the calcite lattice. Recent experimental studies of cation diffusion in calcite (Fisler and Cygan 1999) provide activation energies on the order of 2.9 eV (at 550 to 800 °C) which are in the range appropriate for ionic diffusion processes. However, the energies are significantly smaller than the defect energies calculated here and, therefore, probably represent an extrinsic process controlled by the migration energy of the cation diffusion from an occupied site to a defect site.

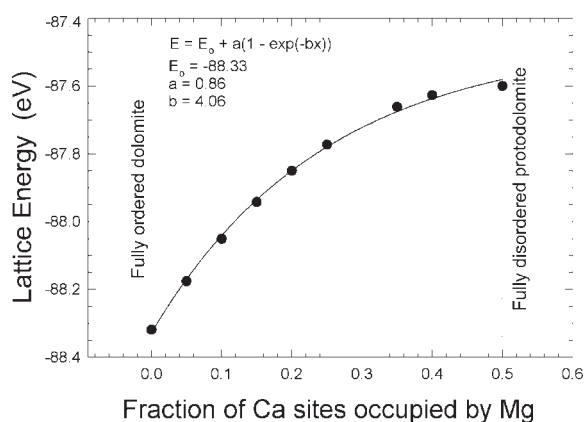


FIGURE 5. Lattice energy for a dolomite-calcite structure as a function of calcium composition and disordering type.

Dolomite disorder types

Ordering energetics in dolomite and the process of dolomitization are still not fully understood. Completely disordered phases preferentially form at low temperatures but are less stable than fully ordered dolomite, which forms rapidly from disordered dolomite (Hardie 1987). Ordering and dolomitization rely on both the driving energies for ordering and on the transport rates for cations in dolomite. Several disorder types for dolomite have been calculated in this study, and may be used to evaluate the ordering mechanisms. Burton (1987) has shown by cluster variation method analysis of carbonate crystals that experimental phase diagrams are reproduced by taking into account highly anisotropic cation ordering, such that interlayer cations highly favor ordering while intralayer interactions favor clustering. The cluster variational model provides a simplistic view of metal interactions based on a tetrahedral cluster and two parameterized interaction terms.

The results of the Mott-Littleton defect model used in the present study provide a more direct measure of the energy penalty for interlayer disorder in dolomite—this is equivalent to the energy of a single anti-site defect, 1.3 eV. By contrast, the energy for forming a single stacking fault (a switch of full magnesium and calcium basal planes) is approximately 0.5 eV, while the energy for an isolated cation substitution is exothermic. These calculations therefore agree that interlayer disorder is energetically disfavored compared to a clustering of cation defects within basal planes. Using varying occupancies for the magnesium and calcium site in a dolomite structure, the carbonate model allows a comparison in lattice energy between fully ordered dolomite and fully disordered (proto-) dolomite. The resulting lattice energy (Fig. 5) can be represented by $E = E_0 + a[1 - \exp(-bx)]$, where x is the fractional occupancy of Mg on the Ca sites. The energy difference between the two fully ordered and fully disordered dolomite (34.4 kJ/mol) represents the driving force for dolomite ordering and compares very well with the enthalpy of disordering (35.76 ± 0.44 kJ/mol) for dolomite measured experimentally by Dooley and Navrotsky (unpublished data).

ACKNOWLEDGMENTS

The authors are grateful for the critical reviews provided by David Price, Lars Stixrude, and an anonymous referee. This paper benefited tremendously from their comments and suggestions. This research was supported by the U.S. Department of Energy, Office of Basic Energy Sciences, Geosciences Research, under contract DE-AC04-94AL85000 with Sandia National Laboratories. Julian Gale also acknowledges the Royal Society for a University Research Fellowship and funding.

REFERENCES CITED

- Borodin, V.L., Lyntin, V.I., Ilyukhin, V.V., and Belov, N.V. (1979) Isomorphic octavite-calcite series. *Soviet Physic Doklady*, 24, 226–227.
- Burton, B.P. (1987) Theoretical analysis of cation ordering in binary rhombohedral carbonate systems. *American Mineralogist*, 72, 329–336.
- Catlow, C.R.A. and Mackrodt, W.C. (1982) *Computer Simulation of Solids*, 320 p. Berlin, Springer-Verlag.
- Catti, M. and Pavese, A. (1997) Quantum mechanical and classical simulations of Mg-Ca carbonates. In B. Silvi and P. D'Arco, Eds., *Modelling of Minerals and Silicated Materials*, 113–156. Kluwer Academic Publishing.
- Catti, M., Pavese, A., and Price, G.D. (1993) Thermodynamic properties of CaCO_3 calcite and aragonite: A quasi-harmonic calculation. *Physics and Chemistry of Minerals*, 19, 472–479.
- Crawford, W.A., and Hoersch, A.L. (1972) Calcite-aragonite equilibrium from 50° to 150° C. *American Mineralogist*, 57, 995–998.
- dal Negro, A. and Ungaretti, L. (1971) Refinement of the crystal structure of aragonite. *American Mineralogist*, 56, 768.

- Dandekar, D.P. and Ruoff, A.L. (1968) Temperature dependence of the elastic constants of calcite between 160 and 300K. *Journal of Applied Physics*, 39, 6004–6009.
- Deer, W.A., Howie, R.A., and Zussman, J. (1966) *An Introduction to the Rock Forming Minerals*. Longmans, London.
- Dick, B.G. and Overhauser, A.W. (1958) Theory of the dielectric constants of alkali halide crystals. *Physical Review*, 112, 90–103.
- Dollase, W.A. and Reeder, R.J. (1986) Crystal-structure refinement of huntite, $\text{CaMg}_3(\text{CO}_3)_4$, with x-ray-powder data. *American Mineralogist*, 71, 163–166.
- Dove, M.T., Winkler, B., Leslie, M., Harris, M.J., and Salje, E.K.H. (1992) A new interatomic potential model for calcite: Applications to lattice-dynamics studies, phase-transition, and isotope fractionation. *American Mineralogist*, 77, 244–250.
- Effenberger, H., Mereiter, K., and Zemann, J. (1981) Crystal structure refinements of magnesite, calcite, rhodochrosite, siderite, smithsonite, and dolomite, with discussion of some aspects of the stereochemistry of calcite-type carbonates. *Zeitschrift für Kristallographie*, 156, 233–243.
- Finger, L.W. (1975) Least squares refinement of the rigid body motion parameters of CO_3 in calcite and magnesite and correlation with lattice vibrations. *Carnegie Institute Washington Yearbook*, 74, 572–575.
- Fiquet, G. and Reynard, B. (1999) High-pressure equation of state of magnesite: New data and a reappraisal. *American Mineralogist*, 84, 856–860.
- Fisler, D.K. and Cygan, R.T. (1999) Diffusion of Ca and Mg in calcite. *American Mineralogist*, 84, 1392–1399.
- Fisler, D.K., Gale, J.D., and Cygan, R.T. (1998) Models of cation diffusion in carbonate minerals. *EOS Transactions of the American Geophysical Union*, 79, S369.
- Gale, J.D. (1996) Empirical potential derivation for ionic materials. *Philosophical Magazine*, 73, 3–19.
- (1997) GULP: A computer-program for the symmetry-adapted simulation of solids. *Journal of the Chemical Society-Faraday Transactions*, 93, 629–637.
- Graf, D.L. (1961) Crystallographic tables for the rhombohedral carbonates. *American Mineralogist*, 46, 238–242.
- Hardie, L.A. (1987) Perspectives: Dolomitization: A critical view of some current views. *Journal of Sedimentary Petrology*, 57, 166–183.
- Hearmon, R.F.S. (1946) The elastic constants of anisotropic minerals. *Reviews of Modern Physics*, 18, 409–440.
- Kay, G.W.C. and Laby, T.H. (1982) *Tables of Physical and Chemical Constants*. Longmans, London.
- Kronenberg, A.K., Yund, R.A., and Gilletti, B.J. (1984) Carbon and oxygen diffusion in calcite: effects of Mn content and PH_2O . *Physics and Chemistry of Minerals*, 11, 101–112.
- Mott, N.F. and Littleton, M.J. (1938) Conduction in polar crystals. I. Electrolytic conduction in solid salts. *Transaction of the Faraday Society*, 34, 485–499.
- Parker, S.C., Titloye, J.O., and Watson, G.W. (1993) Molecular modeling of carbonate minerals: Studies of growth and morphology. *Philosophical Transactions of the Royal Society of London Series A—Physical Sciences and Engineering*, 344, 37–48.
- Pavese, A., Catti, M., Price, G.D., and Jackson, R.A. (1992) Interatomic potentials for the CaCO_3 polymorphs (calcite and aragonite) fitted to elastic and vibrational data. *Physics and Chemistry of Minerals*, 19, 80–87.
- Rao, K.S. and Rao, K.V. (1968) Dielectric dispersion and its temperature variation in calcite single crystals. *Zeitschrift für Physics*, 216, 300–306.
- Ross, N.L. (1997) The equation of state and high-pressure behavior of magnesite. *American Mineralogist*, 82, 682–688.
- Ross, N.L. and Reeder, R.J. (1992) High-pressure structural study of dolomite and ankerite. *American Mineralogist*, 77, 412–421.
- Tosi, M.P. (1964) Cohesion of ionic solids in the Born model. In F. Seitz and D. Turnbull, Eds., *Solid State Physics: Advances in Research and Applications*, 1–120, Academic Press, New York.
- White, W.B. (1974) The carbonate minerals. In V.C. Farmer, Ed., *Infrared Spectroscopy of Minerals*, p. 227–284. Mineralogical Society, London.
- Zhang, J. and Reeder, R.J. (1999) Comparative compressibilities of calcite-structure carbonates: Deviations from empirical relations. *American Mineralogist*, 84, 861–870.

MANUSCRIPT RECEIVED MAY 18, 1998

MANUSCRIPT ACCEPTED SEPTEMBER 8, 1999

PAPER HANDLED BY LARS STIXRUDE